On the relation between >30 keV auroral electron flux and 38.2 MHz radiowave absorption at high latitude.

uclan University of Central Lancashire Centre for Astrophysics

M. J. Birch[1], J. K. Hargreaves[1,2], B. J. I. Bromage[1], D. S. Evans[3]

(1) Centre for Astrophysics, University of Central Lancashire, UK. (2) Department of Communication Systems, Lancaster University, UK
(3) Space Environment Centre, NOAA, Boulder, USA.

uclan University of Central Lancashire Centre for Astrophysics

Introduction

The quantitative relationships between auroral radiowave absorption and energetic electron precipitation have been a topic of interest ever since auroral absorption was recognised as a distinct phenomenon (Reid and Collins, 1959). Early relationships were based on the total electron flux of energy exceeding 40 keV observed on orbiting satellites (Alouette I, Injun I) crossing through, or near to, the field of view of a broad-beam riometer:

$$A = 4.0\times10^{-3}\sqrt{J_{40}} \quad \text{......1a}$$

$$A = 2.0\times10^{-3}\sqrt{J_{40}} \quad \text{......1b}$$

$$A = 3.3\times10^{-3}\sqrt{J_{40}} \quad \text{......2}$$

(Jelly et al., 1964: Equ 1; Parthasarathy et al., 1966: Equ 2). Here, *A* is the 30 MHz absorption (broad beam) in decibels and J_{40} is the electron flux exceeding 40 keV in $cm^{-2}.s^{-1}.sr^{-1}$. Equation 1a is for daytime, 1b is for night, and 2 is for the whole day with the qualification that it was derived for the condition that the flux was almost isotropic.

Imaging riometer data

With the advent of the imaging riometer (Detrick and Rosenberg, 1990), producing beam-widths of only 13^O to15^O (and giving a spatial resolution as small as 20 to 30 km at 90 km altitude), it is possible to reduce the smearing effect of a broad-beam riometer and also to obtain several points of comparison at each overpass.

Figure 1 compares the count rates for electrons of energy exceeding 30 keV (P_{30},T_{30}) observed in the "precipitated" and the "trapped" detectors on NOAA orbiting satellites (POES series), with the 38.2 MHz radio absorption from the imaging riometer at Kilpisjärvi (Browne et al, 1995), the location of which is 69.05^O N, 21.70^O E, L=5.9. The satellites are in sun synchronous orbits at about 850 km altitude and the data are from three sectors of local time: "night" ~03:00 LT, 01:45 UT; "morning" ~08:30 LT, 07:15 UT; and "noon" ~12:15 LT, 11:00 UT. There are 4, 5 and 3 overpasses in these groups, respectively. The detector resolution is 2s, and absorption values were interpolated to corresponding points along the track, which were therefore about 13 km apart, giving 17 or 18 data points per pass. All the selected passes went within 40 km (1^O of longitude) of Kilpisjärvi, and the comparison was only made if the absorption on a broad-beam riometer at the site reached at least 1 dB. Count rates should be multiplied by 100 to convert to flux in $cm^{-2}.s^{-1}.sr^{-1}$.

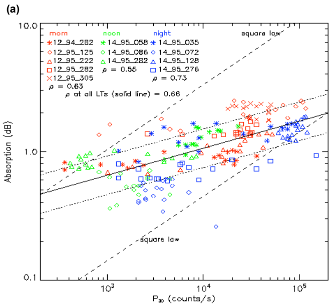

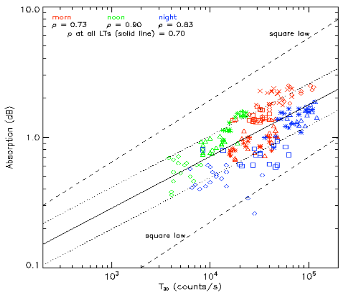

Figure 1(a,b) Variation of 38.2 MHz absorption with (a) precipitated and (b) trapped >30 keV auroral electron flux, for selected passes in the morning, noon and night sectors, showing individual passes grouped in local time by colour, the regression line for the population as a whole (solid lines), standard error limits (dotted lines), and square law 'rails' for comparison (dashed lines).

The regression equations that one would use to predict the absorption (A) from the precipitated (P_{30}) and trapped (T_{30}) count rates are

$$A = 0.153\times P_{30}^{0.210} \quad \text{...... 3a}$$

and

$$A = 0.0185\times T_{30}^{0.396} \quad \text{...... 3b}$$

The standard errors of the estimate are respectively factors of 1.44 and 1.41. Some 2/3 of estimates should be accurate to better than the standard error. The correlation coefficients for the distributions in Figures 1a and 1b are 0.66 and 0.70. For individual local time groups the coefficients range between 0.55 and 0.90.

The "trapped" count rate (which is measured by a detector covering pitch angles from 63^O to 94^O) is a slightly better predictor than the "precipitated" count rate (measured over pitch angles from 2^O to 32^O), but, more significantly, the variation of absorption with count rate is closer to the square-root law expected on physical grounds. As may be seen from Figure 1b, the distribution of data points is close to a square-root law overall (though Equation 3b is the better for prediction purposes). Table 1 shows absorption values estimated from Equations 3a and 3b for sample values of count rate. There is a 68% chance that the true value lies between the values in brackets.

	Absorption (dB)	
Regression against:	P_{30}	T_{30}
Equation	3a	3b
Count rate 10⁴ (/s)	1.06 (0.74 – 1.53)	0.71 (0.50 – 1.00)
Count rate 10⁵ (/s)	1.72 (1.19 – 2.48)	1.77 (1.26 – 2.50)

Table 1: Absorption (dB) at 38.2 MHz predicted from Equations 3.

Inspection of the data from individual passes confirms that the variations in precipitated count rate are considerably greater than one would expect, whereas the variation of trapped count rate is close to that of the absorption squared. An example is shown in Figure 2. We shall therefore prefer the trapped count rates for prediction purposes.

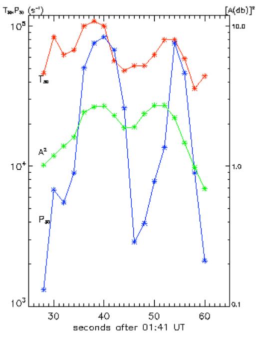

Figure 2: Comparison of $[A(db)]^2$ (green) with P_{30} (blue) and T_{30} (red) count rates, during a pass by NOAA-12 on February 4th 1995

Use of a spectral indicator

The above analysis makes no allowance for variations in the electron spectrum which certainly occur with local time and probably also from case to case at a given local time. The POES detectors give the count rate for electrons >100 keV as well as for >30 keV, and the ratio T_{100}/T_{30} is a measure of spectral hardness. We can also use the parameter

$$E_0 = \frac{100-30}{\ln\left(\frac{T_{100}}{T_{30}}\right)} \quad \text{...... 4}$$

which is the characteristic energy in a spectrum of exponential form $T = T_0 \exp(-E/E_0)$. Since we do not know the shape of the spectrum in the present case we shall call E_0 the "pseudo-characteristic" energy.

For an unchanging spectrum we expect to find $A \propto \sqrt{T_{30}}$. Figure 3 plots $1000A/\sqrt{T_{30}}$ against both T_{100}/T_{30} and E_0. There is a positive correlation in each case, and the regression equations are

$$A = \sqrt{T_{30}}\left(19.5\left(\frac{T_{100}}{T_{30}}\right)+4.15\right)\times10^{-3} \quad \text{...... 5a}$$

and

$$A = \sqrt{T_{30}}\left(0.129E_0+2.43\right)\times10^{-3} \quad \text{...... 5b,}$$

with standard errors $1.73\times10^{-3}\sqrt{T_{30}}$ and $2.23\times10^{-3}\sqrt{T_{30}}$ respectively. The error is somewhat smaller in the first case (Equation 5a), for which some sample values with errors are quoted in Table 2a.

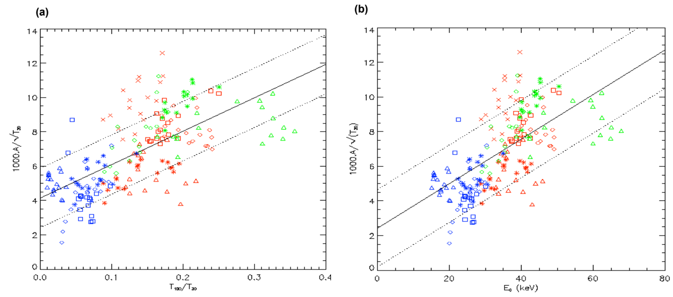

Figure 3: Response of $1000A/\sqrt{T_{30}}$ to changes in (a) the spectral index T_{100}/T_{30}, and (b) the pseudo-characteristic energy E_0,
showing the line of best fit (solid) and the standard error lines (dotted).
(The key for the coloured symbols is given in Figure 1a.)

T_{30} (counts/s)	(a) Linear regression against T_{100}/T_{30}		(b) Logarithmic regression against E_0(keV)	
	0.05	0.20	23.3	43.5
10⁴	0.51 ± 0.17	0.81 ± 0.17	0.50 ± 0.17	0.79 ± 0.27
10⁵	1.62 ± 0.55	2.55 ± 0.55	1.58 ± 0.54	2.49 ± 0.85

Table 2: Absorption predictions from two assumed trapped count rates using (a) linear regression for two selected 'spectral indices' (Equation 5a), and (b) logarithmic regression for two equivalent 'pseudo-characteristic energies (Equation 6b)

Running the regression analysis using *log(* $A/\sqrt{T_{30}}$*), log(*T_{100}/T_{30}*) and log* E_0, gives the equations

$$A = 0.163\sqrt{T_{30}}\left(\frac{T_{100}}{T_{30}}\right)^{0.302} \quad \text{...... 6a}$$

and

$$A = 0.509\times10^{-3}\sqrt{T_{30}}\,E_0^{0.726} \quad \text{...... 6b,}$$

the standard errors being factors of 1.52 and 1.34 respectively. E_0 is now the better predictor, and sample values from Equation 6(b) are given in Table 1(b). There is little to choose between linear regression based on T_{100}/T_{30} and logarithmic regression based on E_0. The former is the better, but only marginally so. The standard errors in Table 2a amount to ±33% and ±21% for T_{100}/T_{30} = 0.05 and 0.20 respectively, which are smaller than those associated with the use of Equation 3 (±40-45%).

Analysis by local-time group

However, the correlation between $A/\sqrt{T_{30}}$ and an index of spectral hardness appears to arise mainly from a variation with time of day. Within a local-time group the correlation is weak, though probably significant for the morning and noon periods. Our third approach is therefore based on the statistics within the three individual groups. The histograms in Figure 4 show the distribution of the quantity $1000A/\sqrt{T_{30}}$ for the night, morning and noon groups. The medians and "standard errors" (which include 2/3 of the values) are summarised in Table 3.

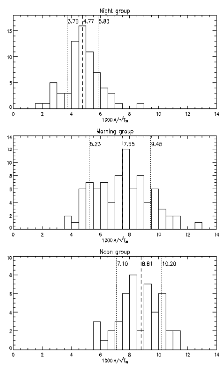

The final columns of Table 3 show the absorption computed using the median values according to the formulae

$$A = 4.77\times10^{-3}\sqrt{T_{30}} \quad \text{...... 7a}$$

$$A = 7.55\times10^{-3}\sqrt{T_{30}} \quad \text{...... 7b}$$

$$A = 8.81\times10^{-3}\sqrt{T_{30}} \quad \text{...... 7c}$$

for the night, morning and noon groups respectively. Standard errors are shown. Comparison of Tables 2 and 3 indicates that this approach is the most accurate of the three, with errors generally below 30%.

It is interesting to note that the ratio between noon and night at a given flux is 1.85, compared with the factor 2 given by Jelly et al. Further, if the formulae of Equation 7 are adjusted for riometer frequency and beam-width, and a pseudo-characteristic energy assumed, they agree with the early formulae (Equations 1 and 2) to better than a factor of 2.

Figure 4: Histograms of $1000\times A/\sqrt{T_{30}}$ for the night, morning and noon groups, showing the median values (dashed) and the standard errors (dotted).

Group	$1000\times A/\sqrt{T_{30}}$			Predicted A(dB) for:	
	Median	SE	SE/median%	T_{30} = 10⁴	T_{30} = 10⁵
Night	4.77	±1.04	22	0.48 ± 0.11	1.51 ± 0.33
Morning	7.55	±2.22	29	0.76 ± 0.22	2.39 ± 0.69
Noon	8.81	±1.54	17	0.88 ± 0.15	2.79 ± 0.47

Table 3: Results of analysis by local time group.

Conclusions

The spatial structure of auroral radio absorption observed with an imaging riometer correlates with the detailed variations of >30 keV flux observed by an orbiting satellite overhead; the observed count rate of trapped electrons may be applied as a predictor of the D-region absorption. The accuracy depends on the prediction method adopted, the standard error being 40-45% if all data are taken together, which may be reduced by taking a form of spectral index into account, and slightly improved further (to 17-29%) by considering each local time sector separately.

References

S. Browne, J.K. Hargreaves and B. Honary. An imaging riometer for ionospheric studies. Electron. Commun. Eng. J. 7, 209 - 215 (1995).
D. L. Detrick and T. J. Rosenberg. A phased-array radiowave imager for studies of cosmic noise absorption. Radio Science 25 (4), 325 - 338 (1990).
D. H. Jelly, I. B. McDiarmid and J. R. Burrows. Correlation between intensities of auroral absorption and precipitated electrons. Can. J. Phys. 42, 2411 - 2418 (1964).
R. Parthasarathy, F. T. Berkey and D. Ventakesan. Auroral zone electron flux and its relation to broad beam radiowave absorption. Planet. Space Sci. 14, 65 - 83 (1966).
G. C. Reid and C. Collins. Observations of abnormal VHF radio wave absorption at medium and high latitudes. J. Atmos. Terr. Phys. 14, 63 - 81 (1959).